Fabrication of Photorefractive Grating With 800 nm Femtosecond Lasers in Fe: LiNbO$_3$ and Rh:BaTiO$_3$ Crystals

Md. Masudul Kabir (D3)

Abstract

Refractive index gratings have been successfully formed in Fe:LiNbO$_3$ and Rh:BaTiO$_3$ crystals using 800 nm femtosecond laser pulses via two-photon and one-photon absorption respectively for the amplification of laser pulses by nonlinear two-wave mixing process. It was confirmed that one-photon absorption is dominant in Fe:LiNbO$_3$ up to 70 GW/cm^2. Chirped grating was formed in Fe:LiNbO$_3$ using amplified high-energy 1 kHz repetition rate femtosecond laser pulses whereas uniform grating was formed in Rh:BaTiO$_3$ using low-energy 76 MHz repetition femtosecond laser pulses. It was found that Rh:BaTiO$_3$ exhibits higher two-wave mixing gain and faster response time than that of Fe:LiNbO$_3$.

1. Introduction

Two-wave mixing (TWM) in photorefractive (PR) crystals have been used for chirp compensation [1], measuring [2-3], temporal storing [4], shaping [5], amplification [6] and self-pumped phase conjugation [7] of ultrashort laser pulses. Grating formation have been carried out with low energy and high repetition rate laser pulses using one-photon and two-photon absorption where multiple pulse effects and cumulative buildup of space-charge electric fields are responsible for the generation of refractive index grating. In BaTiO$_3$ and Fe:LiNbO$_3$ crystals, gratings have been formed either by the interference of Fourier transform limited (FTL) pulses [3,6-7] or by the interference of chirped and the corresponding Fourier transform limited pulses [1-2, 4-5].

However, in these early studies, the role of chirped volume grating for encoding and amplification of broadband optical laser pulses was not explored. Very recently Nishioka *et al.* [8] demonstrated formation of chirped volume grating in Fe:LiNbO$_3$ in order to amplify few cycle femtosecond laser pulses. The PR effects in wide band gap (4 eV) LiNbO$_3$ [9] crystal with femtosecond laser pulses in the near-IR regime can be governed by either linear one-photon or nonlinear two-photon absorption (TPA) using iron impurity centers, depending on the crystal doping concentration and intensity of the writing laser pulses. Although the experimental results of femtosecond laser pulse amplification using chirped volume grating formed in Fe:LiNbO$_3$ at 800 nm by Nishioka *et al* [8] was interpreted based on two-photon absorption, so far there is no research report showing direct evidence of TPA at 800 nm in Fe:LiNbO$_3$. It was intended to amplify 800 nm shaped femtosecond laser pulses generated from a Ti:Al$_2$O$_3$ amplifier via nonlinear TWM process in Fe:LiNbO$_3$. Because the repetition rate of regenerative amplifier is ~ 1 kHz, higher absorption rates are required to form chirped grating in Fe:LiNbO$_3$ within a reasonable writing time. Therefore, it is important to examine whether nonlinear absorption is available at the intensity range of the amplified laser pulses.

Investigation was carried-out to confirm which physical process of light absorption causes the refractive-index changes

in Fe:LiNbO$_3$ upon illumination with 800 nm femtosecond laser pulses up to 400 GW/cm^2 intensity range. It was confirmed that one-photon absorption is dominant in Fe:LiNbO$_3$ up to 70 GW/cm^2. Chirped grating was formed by two-photon absorption in Fe:LiNbO$_3$ by high energy 800 nm laser pulses at a repletion rate of 1 kHz for the amplification of femtosecond laser pulses via TWM.

On the other hand, undoped BaTiO$_3$ crystal is not suitable for grating formation in TWM via one-photon absorption in the near-infrared region because of its low linear absorption in this wavelength regime. Intensive research has been recently conducted to improve the sensitivity of BaTiO$_3$ in the near-infrared region. As a result, a new type of BaTiO$_3$ crystal was grown, blue in color, with rhodium (Rh) as a main dopant. This Rh:BaTiO$_3$ crystal proved to have significantly increased red and infrared absorption in these wavelength regimes [10]. Imaizumi *et al*. [11] first reported amplification of ultrafast laser pulses in 0$^{°}$-cut Rh:BaTiO$_3$ at 1000 nm wavelength using picosecond laser pulses. They also measured phase conjugate reflectivity in their crystal. Nawata *et al.* [12-13] also demonstrated picosecond phase conjugation in 0$^{°}$-cut Rh:BaTiO$_3$ at 1000 nm wavelength.

However, so far there is no research report demonstrating amplification of femtosecond laser pulses in Rh:BaTiO$_3$. Amplification of femtosecond laser pulses in a 0$^{°}$-cut Rh:BaTiO$_3$ crystal at 800 nm wavelength has been demonstrated via TWM process utilizing its high single-photon absorption in the near-infrared region of wavelength.

2. Grating Formation in Fe:LiNbO$_3$ by TWM

2.1 Experiments and Results

2.1.1 Measurement of Light absorption

The measurement of light absorption was performed using a balanced detection technique. Fig. 1 shows the experimental setup for the measurement of light absorption in Fe:LiNbO$_3$ crystal.
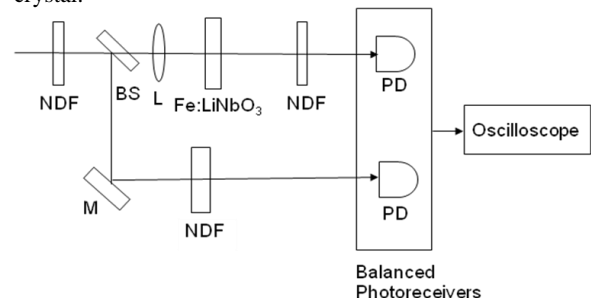

Fig. 1 Experimental setup for measurement of absorption coefficient in Fe:LiNbO$_3$

The laser source was a mode-locked Ti:Al$_2$O$_3$ oscillator, which

generates 30-fs (FWHM) femtosecond laser pulses at 800 nm and at repletion rate of 76 MHz. The spatial spot diameter (at $1/e^2$ intensity level) of the laser beam was ~2 mm. Absorption was measured up to ~5 GW/cm^2 for 76-MHz oscillator pulses. A 2-mm-thick $Fe:LiNbO_3$ (Fe concentration: 0.05 mol%) crystal was used to measure the light-absorption coefficient. The c-axis of the crystal was kept parallel to the light polarization. Absorption of the same crystal was also measured using laser pulses amplified by the regenerative amplifier at 1 kHz at the incident laser intensity ranging from 10 to 388 GW/cm^2. Transmission spectra of the same crystal was also measured shown in Fig. 2.
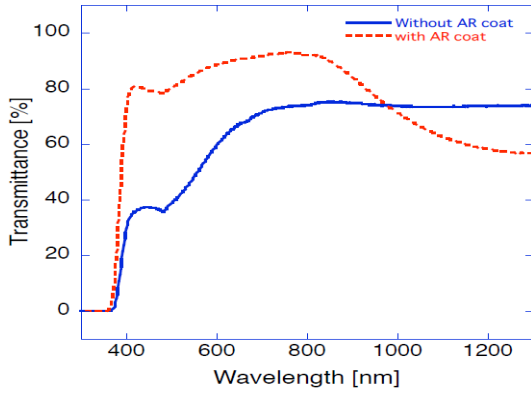

Fig.2 Transmission spectra of $Fe:LiNbO_3$ crystal.

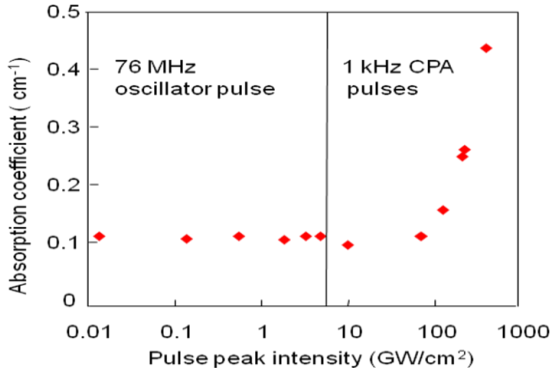Fig. 3 shows experimental results of light absorption coefficient for ordinarily polarized light.

Fig. 3 Absorption of 800-nm femtosecond laser pulses at peak intensity ranging from 15 MW/cm^2 to 388 GW/cm^2 in $Fe:LiNbO_3$.

From Fig. 3 it is observed that up to 70 GW/cm^2, light absorption is almost linear with an absorption coefficient of ~0.11/cm. Above 70 GW/cm^2, a trend of slight increase of absorption coefficient is visible and a sharp increase of absorption starts after 100 GW/cm^2. At around 400 GW/cm^2, the obtained nonlinear absorption coefficient is ~0.34/cm which is ~ 3 times as high as that of the linear absorption coefficient. The nonlinearly absorption starts above 70 GW/cm^2, most probably is due to two-photon impurity-to-band transition by iron ion centers located in the midgap of $LiNbO_3$ crystal. The observed nonlinear absorption may also be

influenced by second harmonic light generated in the crystal in the GW/cm^2 intensity regime.

2.1.2 Grating Formation by 76 MHz and 1 kHz Laser Pulses

Volume phase gratings were formed in the same crystal that was used to measure the absorption coefficient. Figure 4 shows the experimental setup for grating formation by amplified femtosecond laser pulses. The seed laser pulses generated from a $Ti:Al_2O_3$ laser oscillator were amplified by the regenerative chirped pulse amplifier (CPA). The output energy of the amplified laser pulses at the repetition rate of 1 kHz is 0.4 mJ/pulse after pulse compression. The shortest pulse width (FWHM) of the output pulses after the compression is ~50 fs. The amplified laser beam was split into two beams: a strong pump beam (I_p) and a weak signal beam (I_s) by the beam splitter (BS). The signal beam passed through the variable time-delay stage and interfered with the pump beam in the crystal. Before grating recording, spatial overlap of the two writing beams was confirmed by adjusting the mirrors used in the optical path of the pump beam, whereas temporal overlap was confirmed by using an SHG crystal placed in the recording position.
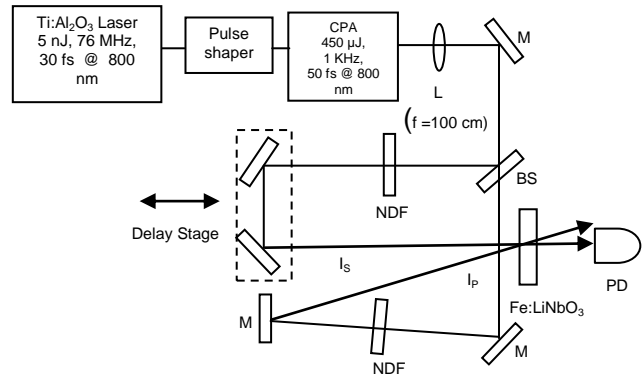

Fig. 4 Experimental setup for monitoring grating formation in TWM experiment. BS: Beam Splitter, M: Mirror, NDF: Neutral density filter, PD: Photo-detector.

A double-path 40-mm-thick fused silica block was used to stretch the temporal width of the pump pulse to 166 fs. NDFs were used to control the power of the writing beams. The writing half-angle of the incident beams was fixed in such a way that a grating spacing of 5.22 µm was formed in the crystal. The pump beam and signal beam entered the crystal symmetrically in a plane containing the c-axis of the crystal so that the grating vector would be parallel to the c-axis of the crystal. The polarization of the writing beams was made parallel to the c-axis of the crystal. The spatial spot diameter (at $1/e^2$ intensity level) of the two beams at the input face of the crystal was kept to 2 mm by inserting a lens of focal length 100 cm. The diffraction efficiency of the pump beam was measured by blocking the signal beam for a short time.

Grating was also formed using the weak oscillator laser beam operated at 76 MHz. The experimental setup was almost the same as that with the amplified laser pulses as shown in Fig. 4. The signal pulse width was stretched by a double-path 40-mm-thick fused silica block from 30 fs to 210 fs.

Gratings were recorded first by low-energy and high-repetition-rate oscillator pulses. Figure 5 shows the time evolution of diffracted signals of the pump beams from gratings recorded by 800-nm femtosecond pulses with a repetition rate of 76 MHz. The average power of a pump beam was 230 mW. The signal beams were 107 mW for the FTL pulses and 85 mW for the stretched pulses (210 fs). During the experiment, it was observed that the diffracted signal from the recorded gratings formed by unstretched pulses is extremely small. For the unfocused recording condition (beam diameter of 2 mm), maximum diffraction efficiency, which was determined from the average power of the diffracted pump beam relative to the incident pump beam power, of ~0.8% was obtained for writing pulse peak intensities of I_p=2.63 MW/cm^2 and I_s=0.11 MW/cm^2. On the other hand, with the stretched signal pulse at I_s=0.0122 MW/cm^2 and the unstretched pump pulse at I_p=2.63 MW/cm^2, a maximum diffraction efficiency of 4.80% was obtained after 1800 sec. For the focused beam recording condition (beam diameter of 0.46 mm), when the signal pulses were not stretched (I_p=58.3 MW/cm^2, I_s=2.44 MW/cm^2), extremely weak diffracted signal was observed at a diffraction efficiency of ~0.8% from the recoded gratings. However, when the signal pulse was stretched (I_p=58.3 MW/cm^2, I_s=0.27 MW/cm^2), a maximum diffraction efficiency of 13.0% was obtained after 600 sec.
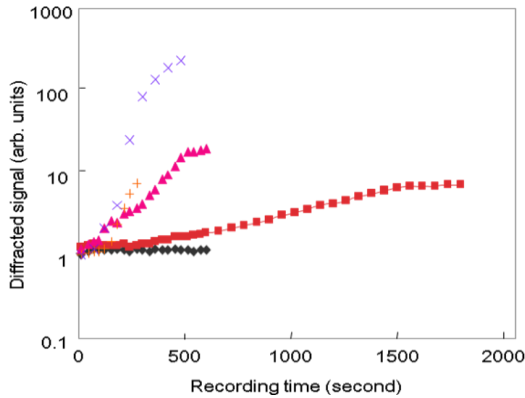

Fig. 5 Time evolution of diffracted signals of the pump beam of 800-nm cw and femtosecond pulse lasers generated from a mode-locked Ti:Al$_2$O$_3$ laser in TWM experiments. The plus and cross plots correspond to cw laser recording with unfocused (I_s=2.5 W/cm^2 and I_p=5.5 W/cm^2) and focused beams (I_s=59 W/cm^2 and I_p=126 W/cm^2), respectively. Diamond and square plots correspond to unstretched (I_s=0.11 MW/cm^2 and I_p=2.63 MW/cm^2) and stretched pulse recording (I_s=0.0122 MW/cm^2 and I_p=2.63 MW/cm^2) with an unfocused beam, respectively. Triangles correspond to stretched pulse (I_s=0.27 MW/cm^2, and I_p=58.3 MW/cm^2) recording for a focused beam.

It was observed that when grating was formed by the continuous laser beams at 800-nm wavelength, the diffraction efficiency was always higher than that of pulse recording for both the unfocused and focused beam recording conditions for a particular recording time with the same average recording power at (I_s=2.5 W/cm^2 and I_p=5.5 W/cm^2) and (I_s=59 W/cm^2 and I_p=126 W/cm^2), respectively, as shown in Fig. 5.

Figure 6 shows experimental results for the time evolution of diffracted signals from the gratings formed by 1 kHz amplified laser pulses generated from the amplifier (CPA).
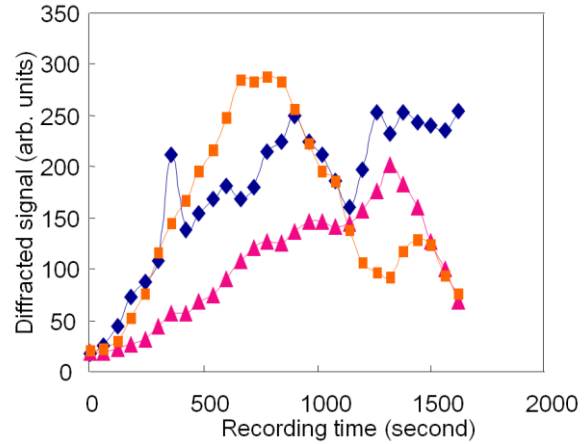

Fig. 6 Time evolution of diffracted signals of the shaped amplified pump beam in TWM experiments. Square plot corresponds to the diffracted signals at I_p = 15 GW/cm^2 and I_s = 31 GW/cm^2 for the pump pulse (166 fs) and signal pulse (50 fs) respectively. Triangle and diamond plots correspond to the results at I_p = 18 GW/cm^2 (166 fs) and I_s = 23 GW/cm^2 (50 fs) and at I_p = 18 GW/cm^2 (166 fs) and I_s = 38 GW/cm^2 (50 fs), respectively.

The highest diffraction efficiency of 17% was obtained when the peak pulse intensities were I_p = 15 GW/cm^2 and I_s = 31 GW/cm^2 for the pump pulse (166 fs) and the signal pulse (50 fs), respectively. When writing peak intensities were changed to I_p = 18 GW/cm^2 (166 fs) and I_s = 23 GW/cm^2 (50 fs) and to I_p = 18 GW/cm^2 (166 fs) and I_s = 38 GW/cm^2 (50 fs), the obtained highest diffraction efficiencies were 10 and 12.6%, respectively. Gratings were erasable and reproducible, and although there were some anomalies in diffraction efficiencies with recording intensities, the trend was similar. There were also some fluctuations in the diffracted signals. Interferometric instability during relatively longer writing time may have caused such fluctuations in the diffracted signals.

Two-wave mixing amplification was carried-out with high-energy laser pulses operated at 1 kHz. The average power ratio of the signal to pump beam was kept to 1:17.4. The average power of the pump pulsed beam was 260 mW, and the pump pulse was stretched from 50 fs to 166 fs by a fused silica block. The average power of the signal beam was 15 mW on the front face of the crystal, while the transmitted power of the signal beam without a pump beam was 14.5 mW. The signal beam was amplified when the both beams were allowed to interfere in the crystal. Fig. 7 shows the time evolution of amplified signal beam in TWM. An amplification of the order 34% was obtained.
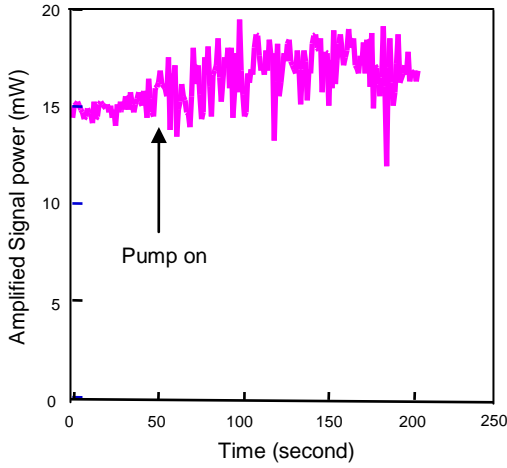
Fig. 7. Time evolution of amplification of signal beam of 800 nm femtosecond laser pulses generated from chirped pulse amplifier in TWM.

The spectrum of the amplified signal pulse is shown in Fig. 8. The amplified signal pulse shifted slightly toward the high-frequency components due to phase-mismatched diffraction of different frequency components from the secondary gratings caused by TWM of different frequency components of the interacting beams.
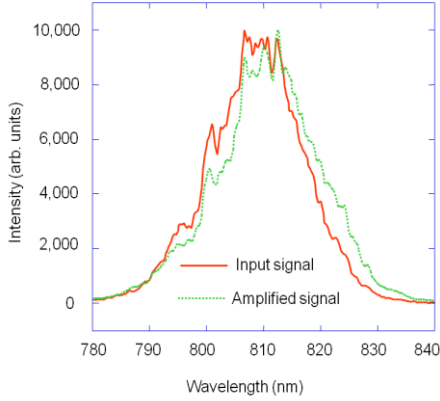

Fig. 8 Input and amplified spectra of signal pulse.

3. Grating Formation in Rh:BaTiO$_3$ by TWM

3.1 Experiments and Results

Two-wave mixing amplification (TWMA) was carried out in an anti-reflection coated Rh:BaTiO$_3$ crystal having a dimensions of 5 x 5 x 4 mm with the c-axis parallel to the 4-mm side. The doping concentration of rhodium in the melt was 400 ppm. The linear absorption coefficient of light measured at 800 nm for the crystal was 1.34/cm. Experimental setup for the measurement of TWMA of low-energy 76 MHz pulses at 800 nm was similar to that shown in Fig. 4. The Fourier transform limited 30-fs (FWHM) pulses were derived from the mode-locked Ti:Al$_2$O$_3$ laser oscillator with the output energy of 5 nJ/pulse. The pulsed laser beam was divided into two beams: a strong pump beam (I_p) and a weak signal beam (I_s) by a beam splitter (BS). φ_s and φ_p are the external angles of incidence for

the signal and pump beam, respectively with respect to the crystal normal. The external crossing angle between the signal and pump beam was fixed at 11° which creates an internal crossing angle of 4° between the beams to form an index grating of spacing Λ = 4.87 μm inside the crystal for all experiments were performed. Orientation of the crystal was varied with a view to optimizing the TWMA gain and minimizing the beam fanning (light-induced scattering) effect to form the angle between the grating vector and c-axis of the crystal ranging at 77°-78°. To minimize the beam fanning, ordinarily polarized light was used as the input beams which forms a slanted grating inside the crystal. The spatial spot diameter (FWHM) of the two beams was adjusted by placing a lens of focal length of 80 cm. Neutral density filter (NDF) was used to adjust the signal to pump beam intensity ratio. TWMA gain measurement was also carried out using 800 nm ordinarily polarized cw laser beams. A power meter was used to measure the power of the amplified signal beam during the TWM experiments. Necessary care was taken by the placing the detector of the power meter far behind the crystal so that scattered light can not reach to the detector during TWMA.

The average input intensity ratio of the signal to the pump beam was fixed to ~1:10 for all the experiments performed. Average power of the signal and the pump beams on the front face of crystal were 15 mW and 157 mW, respectively. The average power of transmitted signal beam in the absence of pump beam was 9 mW, whereas the average power of the transmitted pump beam in the absence of signal beam was 91 mW. Since the spatial extent of the femtosecond pulse laser is of the order of micrometers, to achieve maximum TWMA gain, measurements were performed first by keeping the beam overlapping width $H = w_0/\cos\theta$ of the two pulsed beams smaller than the grating width $W = c\tau/n\sin\theta$ formed by the two interfering pulses inside the crystal, where w_0 is the incident beam width, c is the speed of light in the vacuum, τ is the pulse duration in the crystal, n is the refractive index of BaTiO$_3$ for ordinary polarized light and θ is the writing half-angle inside the crystal. When the two beams were allowed to interfere in the crystal, the power of the signal beam increased while the power of the pump beam decreased. The direction of power flow between the two beams was reversed when the crystal's c-axis was inverted. Figure 9 shows the temporal evolution of the amplified signal beam for different incident beam angles for the beam overlapping width H = 0.1 mm [FWHM] and the grating width W = 0.3 mm [FWHM].
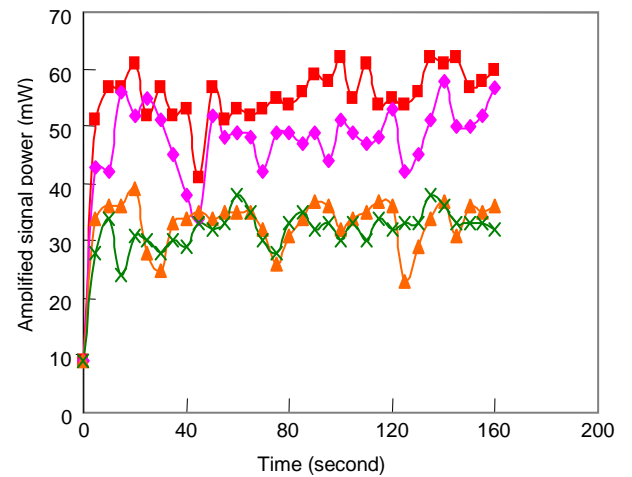
Fig. 9 Time evolution of amplification of signal beam of 800 nm femtosecond pulse laser generated from a mode-locked Ti:Al$_2$O$_3$ laser in TWM in Rh:BaTiO$_3$ for 1:10 signal (I_s =180 W/cm^2) to pump beam (I_p = 1884 W/cm^2) average intensity ratio for different incident beam angle. W/H=0.3/0.1. Diamond, square, triangle and cross plots correspond to the amplifications of signal beam for 24°, 25°, 26° and 27° angles of incidence of signal beam on the crystal surface.

From Fig. 9, we can see that the average power of the signal beam increases with time until reaching an approximately steady state value. The fluctuations in the amplified signal beams are due to beam fanning from the signal beam itself. The value of maximum gain for signal beam for different incident angles is somewhat different but the trend of time evolution of amplified signals is similar for all measurements. The maximum gain of 6.44, 6.88, 4.33 and 4.22 were obtained when the signal beam was incident at 24°, 25°, 26° and 27° on the crystal front face, respectively.

To investigate the role of the geometric factors concerning grating width and the beam overlapping width that influence the femtosecond TWMA process, TWMA gain of signal beam was measured by keeping the beam overlapping width ~ 2 times larger than that of the grating width [H = 0.55 mm (FWHM), W = 0.3 mm (FWHM)]. The average power of signal and pump beam on the front face of crystal were 21.5 mW and 215 mW, respectively. The average power of the transmitted signal and pump beams in the absence of grating were 10 mW and 108 mW, respectively in this experiment. Figure 10 shows the time evolution of the amplified signal beams for different incident beam angles.
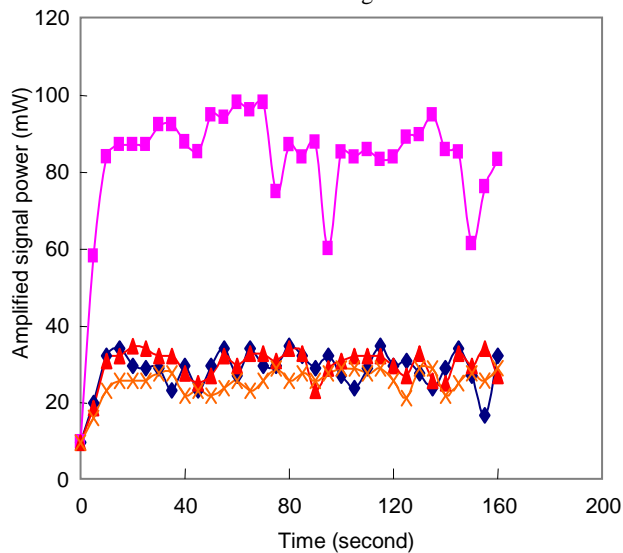

Fig. 10. Time evolution of amplification of signal beam of 800 nm femtosecond pulse laser generated from a mode locked Ti:Al$_2$O$_3$ laser in TWM in Rh:BaTiO$_3$ for 1:10 signal (I_s = 9 W/cm^2) to pump beam (I_p = 90 W/cm^2) average intensity ratio for different incident beam angle. W/H=0.3/0.55. Diamond, square, triangle and cross plots correspond to the amplifications of signal beam for 24°, 25°, 26° and 27° angles of incidence of signal beam on the crystal surface.

At the incident beam angles except for 25°, the obtained maximum gains were ~2.9-3.5. These gains are smaller than those obtained with the small beam overlapping width (H = 0.1 mm) in Fig. 9. A maximum gain of 9.8 was obtained when the signal beam was incident at 25° on the crystal front face.

TWMA gain was also measured in the same crystal using cw laser at 800 nm keeping the beam overlapping width H = 0.55 mm that was used for femtosecond TWMA gain measurement. In this experiment, the average power of signal and pump beam on the front face of crystal were 21 mW and 210 mW, respectively. The average power of transmitted signal and pump beams were 11 mW and 114 mW, respectively in the absence of grating. Figure 11 shows the time evolution of amplified signal beam of cw laser.
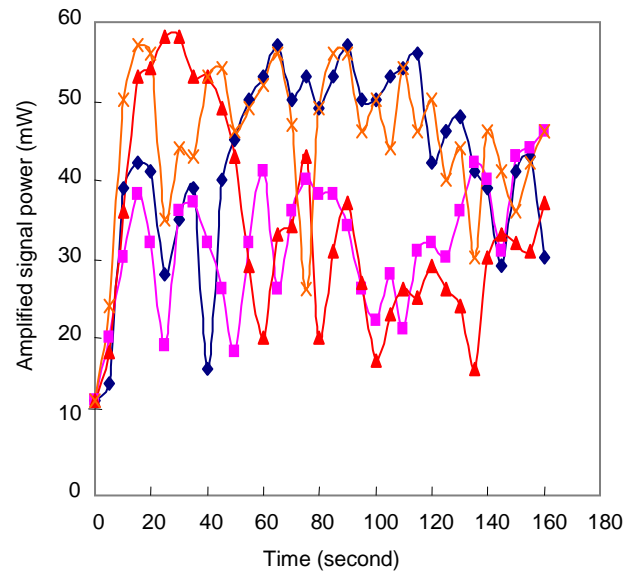

Fig. 11. Time evolution of amplification of signal beam of 800 nm cw laser generated from a mode-locked Ti:Al$_2$O$_3$ laser in TWM in Rh:BaTiO$_3$ for 1:10 signal (I_s =8.8 W/cm^2) to pump beam (I_p = 88 W/cm^2) intensity ratio for different crystal orientations. Diamond, square, triangle and cross plots correspond to the amplifications of signal beam for 24°, 25°, 26° and 27° angles of incidence of signal beam on the crystal surface.

In this case, for all incident angles except 25°, the maximum measured gain reached ~5. At 25° angle of incidence of signal beam, the obtained gain was slightly lower at 4. The severe fluctuations and gradual reduction of amplification with time in the amplified signal beams can be attributed to the strong beam fanning arising from both the pump and signal beams.

The spectra of the input and amplified femtosecond signal pulses were also recorded as shown in the Figs. 12 (a) and 12 (b).
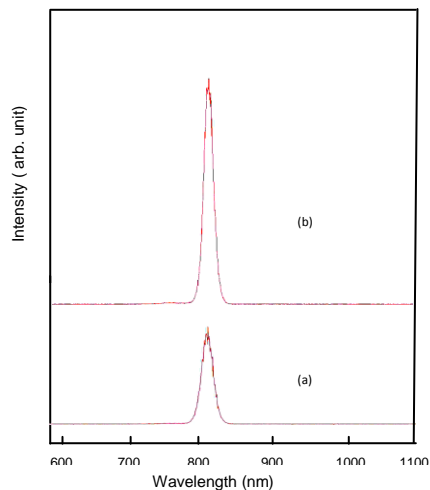
Fig. 12 Spectrum of the signal pulse: (a) before the crystal front surface and (b) amplified signal pulse by TWM in Rh:BaTiO$_3$.

The profile of both spectra are same with the spectrum width of ~ 20 nm (FWHM) which means that there is less phase-mismatching in diffraction of different frequency components of the pulse while they diffracted from the gratings formed by the frequency components other than their own frequency components.

4. Conclusion

Volume phase gratings were formed using 1 kHz high-energy and 76 MHz low-energy femtosecond laser pulses in Fe:NiNbO$_3$ and Rh:BaTiO$_3$ crystals respectively via two-wave mixing process. Grating was formed in Fe:LiNbO$_3$ by two-photon absorption which appears at pulse peak intensity > 70 GW/cm^2 where the measured linear absorption coefficient in the crystal was ~ 0.11/cm at 800 nm. On the other hand, gratings were formed in Rh:BaTiO$_3$ by one-photon absorption having a linear absorption coefficient of ~ 1.34/cm at 800 nm. It was found that Rh:BaTiO$_3$ is more efficient photorefractive crystal than Fe:NiNbO$_3$ for the amplification of femtosecond laser pulses at 800 nm wavelength because of its higher two-wave mixing gain and faster response time compared to Fe:NiNbO$_3$.

References

[1]   M. L. Roblin, F. Gires, R. Grousson, and P. Lavallard: Opt. Commun. 62, 209 (1987).
[2]   V. Dominic, X. S. Yao, R. M. Pierce, and J. Feinberg, Appl. Phys. Lett. 56, 521 (1990).
[3]   R. Trebino, C. C. Hayden, A. M. Johnson, W. M. Simpson, and A. M. Levine, Opt. Lett. 15, 1079 (1990).
[4]   L. H. Acioli, M. Ulman, E. P. Ippen, J. G. Fujimoto, H. Kong, B.S. Chen, and M. Cronin-Golomb, Opt. Lett. 16, 1984 (1991).
[5]   X. S. Yao, and J. Feinberg, Opt. Lett. 18, 622 (1993).
[6]   M. Horowitz, B. Fischer, Y. Barad, and Y. Silberberg, Opt. Lett. 21, 1120 (1996).
[7]   C. Yang, K. Minoshima, K. Seta, H. Matsumoto, and Y. Zhu, Appl. Opt. 38, 1704 (1999).
[8]   H. Nishioka, K. Hayasaka, S. Ohta, H. Tomita, and K. Ueda, Opt. Express, 15, 4830 (2007).
[9]   O. Beyer, I. Breunig, F. Kalkum, and K. Buse, Appl. Phys. Lett. 88, 051120 (2006).
[10]   B. A. Wechsler, M. B. Klein, C. C. Nelson, and R. N. Schwartz, Opt. Lett. 19, 536 (1994).
[11]   T. Imaizumi, M. Goto, Y. Ojima, and T. Omatsu, Jpn. J. Appl. Phys. 43, 2515 (2004).
[12]   K. Nawata, Y. Ojima, M. Okida, T. Ogawa, and T. Omatsu, Opt. Express, 14, 10657 (2006).
[13]   K. Nawata, M. Okida, K. Furuki, and T. Omatsu, 15, 9123 (2007).